PCCP

Formation of chains of graphitic nanoparticles by heating fullerene blacks covered with thin metal films

H. Kanzow,*†[a] A. Ding,[a] J. Nissen,[b] H. Sauer,[c] T. Belz[c] and R. Schlögl[c]

[a] *Optisches Institut, TU Berlin, Sekr. P1-1, Str. d. 17 Juni 135, D-10623, Berlin, Germany*
[b] *Zentraleinrichtung Elektronenmikroskopie, TU Berlin, Sekr. KWT 2, Str. d. 17 Juni 135, D-10623, Berlin, Germany*
[c] *Fritz-Haber-Institut der Max-Planck-Gesellschaft, Faradayweg 4-6, D-14195, Berlin, Germany*

Received 6th April 2000, Accepted 27th April 2000
Published on the Web 24th May 2000

Strongly bent, fibrous carbon nanostructures with outer diameters usually between 35 and 90 nm were generated by the pyrolysis above 800 °C of a fullerene black which had been covered with a thin nickel film. Transmission electron microscopy (TEM) and electron energy loss spectrometry (EELS) revealed that the material consists of chains of hollow elongated multi-wall graphitic nanoparticles. The worm-like nanostructures only arose from the nickel-covered parts of the fullerene black as checked with scanning electron microscopy (SEM) and energy-dispersive X-ray spectrometry (EDX). Attempts to generate similar structures from commercial carbon blacks, arc-produced fullerene-free carbon blacks and glassy carbon failed. Substituting nickel by cobalt or molybdenum also did not lead to the generation of fibrous structures. Additionally, the pyrolysis-induced changes of metal films on graphite and glassy carbon and the direct interaction of nickel films with fullerene vapour were investigated. A growth model for the nanochains is proposed, which includes the diffusion of carbon through a metal particle, the segregation of carbon and the repeated surface melting and solidification of the metal.

1. Introduction

In the Krätschmer–Huffman method,[1] pure graphite electrodes are evaporated with an electric arc in a noble gas atmosphere. By controlling the reaction parameters carefully, a "soot"-like material with a high percentage of extractable fullerenes can be produced.[2,3] Covaporisation of catalytic metals with carbon led to the discovery of single-wall carbon nanotubes (SWCNT).[4,5] Different mechanisms for the formation of SWCNTs from carbon–metal plasma were proposed[6,7] and theoretical studies[8–11] have been performed. However, due to the lack of direct observation of the formation of different nanostructures from the plasma, there is still no experimental proof for the different theoretical models.

Besides isolated nanoparticles which are usually present in the cathode deposit of pure carbon arcs, chains of hollow multi-wall graphitic nanoparticles were observed when nickel or iron had been used as catalysts.[12,13] The interconnected particles were almost spherical, with outer diameters of 10–20 nm and inner diameters up to 10 nm. Some of the graphitic particles of the chains were filled with the metal that was used as the catalyst. Cobalt was also tried, but surprisingly failed to produce nanochains.

Multi-wall carbon nanotubes (MWCNTs) and less crystalline carbon nanofibres have been known for a long time.[14–16] They are usually produced by chemical vapour deposition (CVD) techniques, where they are formed during the decomposition of hydrocarbons on metal catalysts.[14–19] Intensive studies in the 1970s led to the establishment of the diffusion model for the growth of MWCNTs from carbon-containing gases.[17] The idea originated from the vapour–liquid–solid (VLS) mechanism developed by Wagner and Ellis for the formation of solid "whiskers" at small metal particles.[20] Tibbetts explained why "whiskers" made of carbon should preferably form MWCNTs.[17] The whisker model does not require explicitly hydrocarbons for the growth of MWCNTs. Indeed branched segmented carbon nanofibres were produced in CVD experiments from fullerene vapour using small iron, cobalt and nickel particles as catalysts.[21] Heating of a sandwich consisting of alternating thin films of nickel and C_{60} to 950 °C led to nickel-filled needle-like MWCNTs.[22]

The processes outside the carbon–metal plasma in the electric arc experiment are certainly very complex as indicated by the variety of products. A first (oversimplified) approximation is given by the phase diagram. The binary alloy diagrams of carbon with the standard catalysts (nickel or cobalt) consist of simple eutectics, with a small solubility of carbon in the metal and a very limited solubility of the metal in the graphitic carbon phase.[23] The metals do not form stable carbides; *e.g.* decomposition of Ni_3C occurs above 430 °C,[24] Co_2C at about 400 °C.[25] According to the phase diagrams we expect carbon-rich carbon–nickel or carbon–cobalt vapours to condense as liquid droplets as the first step after leaving the hot plasma. Further cooling results in the segregation of a metal-free carbon phase from the liquid. Finally a metal-rich phase will be deposited on these carbon particles. They float in the gas phase of the reactor and may get attracted and finally deposited onto the hot cathode. Most of this carbon is amorphous.[5,12,13] However, amorphous carbon can be transformed into graphite at temperatures above 500 °C in the presence of nickel or cobalt.[25,26] We designed a simple experiment to test

† Present address: Groupe de Dynamique des Phases Condensées, Université de Montpellier II, CC 26, 34095 Montpellier Cedex 05, France.

if arc-produced carbon in contact with metal tends to undergo secondary reactions, especially if carbon nanotubes can be made in this way.

2. Experimental

Four different fullerene black samples (FB1–FB4) were produced in a helium atmosphere by vaporisation of graphite with an electric arc in a commercial reactor (Bucky II, Ulvick Industries) according to the Krätschmer–Huffman method. As the experimental details and the characterisation of the materials with high-resolution transmission electron microscopy (TEM), powder X-ray diffraction and thermogravimetric analysis/differential thermal analysis (TGA/DTA) are described elsewhere,[3,27] only short descriptions for the different materials are given:

FB1 is a typical fullerene black, with a fullerene content of approximately 10% (confirmed by high-performance liquid chromatography, HPLC). The helium pressure was 400 mbar. The material is highly amorphous.

FB2 is a mixture of fullerene blacks similar to FB1. The samples originally contained 4.5 to 7% of fullerenes, which had been removed with refluxing toluene.

FB3 was prepared under 0.1 mbar helium. This sample did not contain any fullerenes (unfavourable production conditions) and was the most graphitic one.

FB4 was prepared under flowing nitrogen conditions (400 mbar). It contained 3.6% N (confirmed by X-ray photoelectron spectroscopy, XPS and elemental analysis), but no fullerenes. It has a characteristic cyanic smell.

Samples containing carbon blacks Fl 101, CN 220 and FW2 (Degussa-Huels), pieces of glassy carbon (Sigradur G, HTW) and graphite (Edelgraphit) were also used for comparison. The powders were pressed into pellets of approximately 10 mg. The pellets were covered with thin sputtered films of nickel (>99%, Gemmel, Berlin), cobalt (>99.9%, Goodfellow, Bad Nauheim) or molybdenum (>99%, Osram, Berlin) and subsequently heated under argon to between 400 and 1200 °C at atmospheric pressure and a gas flow of 115 cm min^{-1}. Before and after the pyrolysis the surfaces of the samples were examined with scanning electron microscopy (SEM) with a Hitachi S-2700 operated at 20 keV. The internal structure of the fibrous material which had formed on the pellets was investigated with a Philips CM200FEG electron microscope operated at 200 keV and equipped with a Gatan GIF100 imaging filter. Specimens for TEM and electron energy loss spectrometry (EELS) analysis were prepared by gently brushing the loose material from the surfaces of the pellets and dusting it directly onto TEM grids covered with lacey carbon films (Plano).

EELS spectra were measured in the low energy loss range up to 150 eV and at the carbon K edge with a large spectrometer acceptance angle of 100 mrad at an energy resolution of 1 eV. In the image mode of the microscope using a magnification of 50 000, areas of approximately 20 nm diameter could be selected on the specimen for EELS analysis.

3. Results

3.1 Fullerene-containing fullerene black FB1

The surface of an FB1 pellet consists of round amorphous carbon particles with diameters of predominantly 50 to 100 nm before pyrolysis (Fig. 1). When no metal was present we did not register any modification with SEM after heating it for 10 min to temperatures up to 1200 °C. A dramatic change was discovered when nickel-coated F01 pellets were heated to sufficiently high temperatures. The surfaces became covered with worm-like nanostructures (Fig. 2). The strongly bent fibrous structures were usually more than 1 μm in length. TEM revealed that the "fibres" are chains of elongated, hollow graphitic nanoparticles with multi-walled shells. Their three-dimensional structure was verified by tilting them to ±40° about their long axis. Usually there was no noticeable difference in the diameter of the units in one chain. However the diameters of the different chains in different samples were between 30 and 430 nm; most common was the range between 35 and 90 nm.

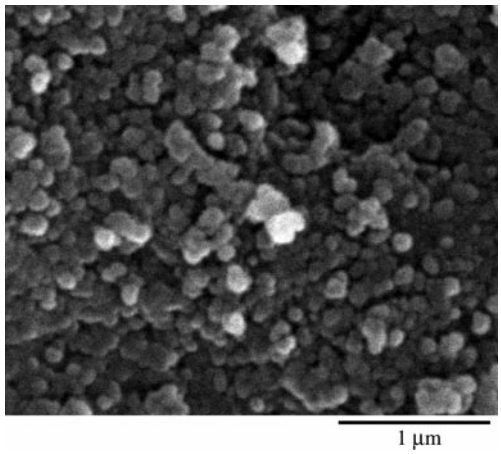

Fig. 1 SEM: surface of FB1 pellet covered with 25 nm of nickel before heating.

Fig. 3 shows a low-magnification image of a chain of very large particles. The outer diameter of this chain was approximately 300 nm and the wall thickness 30 nm. Most of its particles were longer than 1 μm. The abrupt change in the image contrast at the inner side of the shell indicates that the particles are hollow. The shells mostly had a corrugated appearance and sometimes the thickness varied clearly even within one chain compartment, especially close to the strongly deformed contact area of two neighbouring particles. Fig. 4 shows a high-resolution image of such a region with more than 90 continuously bent graphite planes with a constant interlayer spacing of 0.34 nm. This interlayer distance was preserved in the straighter middle sections of the particles, when they were tilted to large angles about their long axes, indicating a more or less circular cross section resembling that of multi-walled carbon nanotubes.

The chains observed with TEM were apparently shorter than the ones visualised with SEM. This is tentatively explained by the breakage of the chains due to mechanical stress in the course of the TEM preparation as the attractive forces between the interlinked chain segments are probably rather weak. Several chain fragments were terminated by

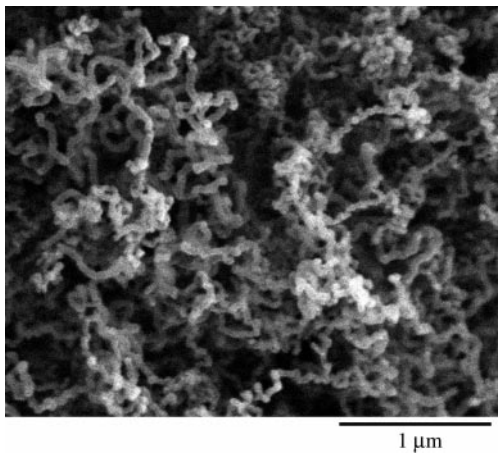

Fig. 2 SEM: surface of FB1 pellet covered with 25 nm of nickel and subsequently heated for 3 min to $T = 1000$ °C.

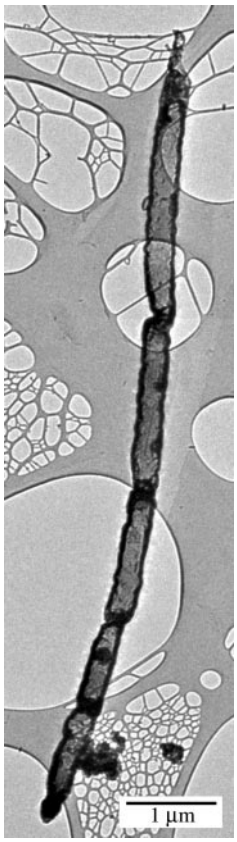

Fig. 3 Low-magnification TEM of a chain of very large nanoparticles.

torn-up particles with open ends. In some of the nanoparticles small nickel clusters with diameters of around 5 nm could be identified by EELS, which were probably left behind from larger metal aggregates during the growth process. Occasionally, isolated large nickel particles encapsulated by multi-walled graphitic shells were found.

For the EELS investigation the chain depicted in Fig. 3 was chosen in order to obtain local information from the different regions of individual particles. With the long axis of a single particle perpendicular to the electron beam, areas in the central part and in the multi-wall region were probed. The

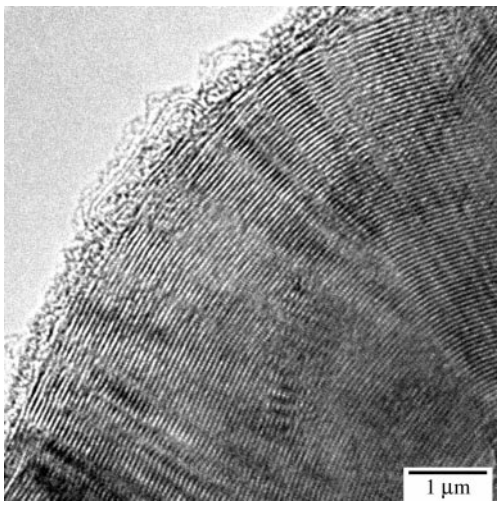

Fig. 4 High-resolution TEM image of the multi-wall region near the contact area of two particles of the chain depicted in Fig. 3 consisting of about 90 continuously bent graphene layers; interlayer spacing ~0.34 nm.

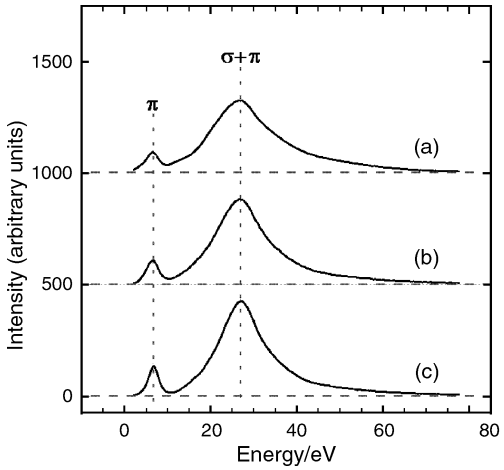

Fig. 5 Low energy loss spectra (EELS) from (a) the multi-wall and (b) the central region of a graphitic nanoparticle and from (c) HOPG, orientated with the *c*-axis parallel to the electron beam. In order to present the π plasmon peak clearly, the zero-loss peak was extrapolated beyond the energy loss region and subtracted. The spectra were Fourier transform deconvoluted to remove the contributions of multiple inelastic scattering and scaled to the same integrated intensity in the energy range shown.

low EELS spectra are shown in Fig. 5 together with the low-loss spectrum taken from highly ordered pyrolytic graphite (HOPG), orientated with the *c*-axis parallel to the electron beam. The HOPG spectrum exhibits the characteristic ($\pi + \sigma$) plasmon at 27.0 eV and a sharp π plasmon peak at 6.8 eV. Apart from minor differences all three spectra look quite similar, showing the graphitic nature of the nanoparticles. From the ratio of the integrated intensities in the zero-loss peak (extrapolated beyond the EELS spectrum and subtracted in Fig. 5) and in the total spectrum and from the knowledge of the mean free path for 200 keV electrons in carbon, the sample thickness can be estimated.[28] This gave a value of about 60 nm for the thickness in the central region, which is twice the mean wall thickness seen at the edge of the particle, giving evidence that it is mainly empty. For the edge position this procedure gave a thickness of about 140 nm, which can be explained under the assumption that the wall of the nanoparticle is built from tubular concentric graphene layers and taking into consideration that the spectra represent an average over a cylindrical volume along the electron-beam direction.

The carbon K edges taken from the multi-wall region and the central part of a graphitic particle are shown in Fig. 6 together with the carbon K edge from HOPG. All the spectra exhibit a leading peak at ~285 eV corresponding to C $1s \rightarrow \pi^*$ transitions. The following broad peak between 290 and 310 eV is mainly due to transitions from C $1s \rightarrow \sigma^*$ states. The scattering geometry (large spectrometer acceptance angle) mostly confines the scattering wave vector to lie in a plane perpendicular to the incident electron beam. For HOPG measurement, this is the basal plane of graphite and therefore a small leading π^* is followed by dominating transitions to σ^* states. Taking the nanoparticle to be built from tubular concentric graphene layers, the wall in the central region has the same orientation to the electron beam and the spectrum [Fig. 6(b)] closely resembles the HOPG carbon K edge in the π^*/σ^* intensity ratio as well as in the characteristic intensity modulation of the σ^* peak (which is, however, less pronounced because of the curvature of the graphene layers and imperfections in the graphitic ordering). For the wall region the scattering wave vector is approximately parallel to the graphite *c*-axis and the intensity of the π^* peak is markedly increased [Fig. 6(a)]. Most experiments of the combination FB1 with nickel are shown in Table 1.

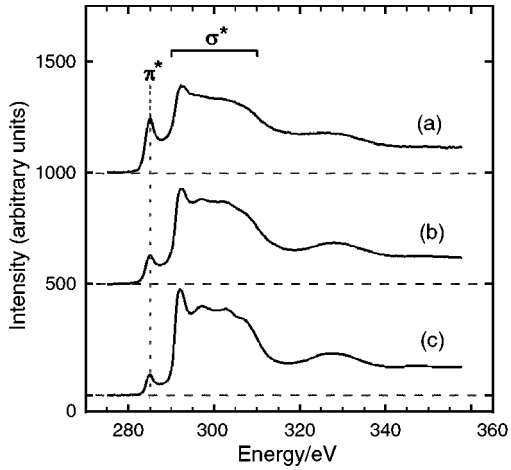

Fig. 6 Background-subtracted carbon K spectra (EELS) from (a) the multi-wall and (b) the central region of a graphitic nanoparticle and from (c) HOPG. The spectra were Fourier transform deconvoluted with the low energy loss spectrum to remove the contributions of multiple inelastic scattering. The spectra are from the edge onset.

The carbonaceous structures observed after heat treatment were not influenced by the reaction time for a time ranging from 1 to 20 min. Likewise, we always observed the same type of worm structure when we varied the nickel film thickness from 2 to 100 nm. To learn more about the reaction, we also varied the oven temperature from 400 to 1200 °C in steps of 50 °C. Between 850 and 1200 °C the same structures as in Fig. 2 were generated. However, at 800 °C the pellets were only poorly covered with fibrous material. These fibres were shorter (~1 μm) and also much thicker (diameters 80–190 nm) than the ones grown at higher temperatures. Below 800 °C no fibres were produced.

Surprisingly we also did not produce any nanofibres (except for single species) by pyrolysis when we were using cobalt instead of nickel with the FB1 pellets. This was also true for molybdenum, but after the heat treatment a material with cauliflower-like appearance covered the surfaces of the pellets.

3.2 Fullerene blacks FB2 and FB3 and carbon blacks FB2, FB3, FW2, Corax N 220 and Fl 101

Pyrolysis for 3 min at 1000 and 1200 °C partially converted the nickel films (25 nm) on the (extracted) fullerene black FB2 and on the carbon blacks FW2 and Corax N 220 into multi-faceted metal-rich particles (energy-dispersive X-ray spectrometry, EDX) with diameters between 100 and 500 nm. However, no change of the surface structure of the nickel-covered FB3 and the Fl 101 pellets were observed with SEM after the same temperature treatment. These results may be due to the difficulty of distinguishing metal and carbon particles with SEM, if they have similar sizes and shapes.

Small metal-rich particles (90–170 nm) were generated from 10 nm cobalt films on all the sooty materials when the pellets were heated for 3 min at 1200 °C. When we used molybdenum (10 nm), 3 min of heating at 1000 °C did not result in any change of the different surfaces. With these carbon materials we have never succeeded in producing any fibres.

3.3 The importance of evaporable fullerenes for the nanochain formation

The following two experiments were carried out to determine if the fibrous nanostructures (Fig. 2) were generated due to the fullerene content in the fullerene black FB1 or by a reaction of nickel with solid amorphous carbon.[25]

Therefore we removed all volatile compounds like fullerenes from FB1 by heating it in argon to 1200 °C for 15 min at ambient pressure. The UV spectrum of the toluene extract of a part of this material confirmed that the removal or destruction of the fullerenes had been complete. Some of these fullerene-free pellets were covered with nickel (25 nm) and subsequently heated for 3 min to 1000 °C. No change in the surface structure was observed. Another part of the fullerene-free FB1 material was mixed with 8 wt.% of C_{60} (Gold grade, Hoechst). These pellets were covered with nickel and pyrolysed as described. The latter showed the same typical worm-like nanostructures as shown in Fig. 2.

3.4 Nitrogen-containing fullerene-free fullerene black FB4

Fibrous surface species in low densities were also synthesised on the surfaces of the nitrogen-containing soot FB4 using nickel (25 nm) or cobalt (10 nm). The samples were heated for 10 min to 1200 °C. The fibres from nickel were about 1 μm long and had diameters of 70–160 nm. The fibres from cobalt were usually less than 1 μm long and their diameters varied between 50 and 100 nm. They appeared to be smoother than the ones produced with nickel. No change of the surface structure was observed in the molybdenum experiments.

3.5 Behaviour of metal films on graphite and glassy carbon

In Section 3.2 we have already mentioned the difficulty of distinguishing metal and sooty carbon particles with SEM, if they have similar sizes and shapes. On plane surfaces it is much easier to study the transformation of the metal films. The graphite was intended to act as an inert carbon substrate (comparable with FB3), while the glassy carbon should simulate a more reactive amorphous material like FB1.

A 25 nm layer of nickel, cobalt or molybdenum was sputtered onto graphite. The samples were heated for 3 min in argon to temperatures between 400 and 1200 °C. Before the pyrolysis the nickel and the cobalt films showed a fine-grained structure in SEM pictures with mean particle diameters lower than 30 nm. With increasing temperatures the structure of the films roughened to mean particle sizes between 30 and 50 nm at 500 °C and between 50 and 90 nm at 800 °C. The particles appeared increasingly separate, but remained a closed layer covering the whole graphite surface. However, at 900 °C a process resembling melting appeared to start: Big islands of metal were built up in such a way that the original carbon surface became partly uncovered. At higher temperatures the metal films were transformed into big, separate, almost spherical, at 1100 and 1200 °C often multi-faceted, metal particles. The cobalt and nickel structures we observed with SEM did not significantly differ for these two metals, when samples of the same pyrolysis temperature were compared. However, the finely structured molybdenum films only started to become

Table 1 Series of experiments with nickel-covered FB1 pellets. The parameters shown in bold were those varied

Reaction series number	1	2	3
Time of pyrolysis/min	**1–20**	3	3
Ni film thickness/nm	25	**2–100**	25
Temperature/°C	1000	1000	**400–1200**
Results	always nanochains	always nanochains	nanochains for $T \geqslant 800$ °C

granular between 700 and 800 °C while the average particle size increased. Above 900 °C small parts of the graphite surface became uncovered. At 1100 °C a further dramatic change occurred, whose result became clear at 1200 °C. Instead of nearly spherical particles, elongated and branched flat forms of the metal were generated.

The nickel films on glassy carbon only became slightly roughened when heated for 3 min to 600 °C. Between 700 and 1000 °C the roughening increased intensely, indicating a reaction between the metal and the glassy carbon. Above 1100 °C a process resembling melting resulted in the formation of metal droplets. The glassy carbon surfaces only seemed to have been slightly etched at these high temperatures. The cobalt film also transformed into droplets after having been heated for 3 min to 1200 °C. Lower temperature experiments were not carried out with cobalt. The molybdenum films did not change when heated up to 1200 °C.

3.6 Interaction of thin nickel films with C_{60} fullerene vapour

These experiments were intended to examine if the solid material of fullerene black FB1 is necessary to generate the nanochains, or if they can also be produced on other substrates.

C_{60} fullerene (100 mg) was vaporised in flowing argon and passed by laser-deposited thin nickel films on quartz at temperatures between 700 and 1200 °C. The preliminary results suggest that there is only a small temperature window between 800 and 1000 °C where fibrous material is formed.[29]

We also studied the reaction of C_{60} fullerene vapour in flowing argon with thin sputtered nickel films on different substrates under various experimental conditions. Very few nanochains were generated when a graphite substrate covered with 25 nm of nickel was introduced into the hot tube reactor at 1200 °C, and shortly afterwards 100 mg of C_{60} fullerene was inserted upstream. The sample stayed inside the hot area for 3 min.

4. Discussion

With the exception of the nitrogen-containing fullerene black FB4 it was proven that evaporable fullerenes and not amorphous carbon represented the main feedstock for the chains of hollow graphitic nanoparticles in our study. This is in accordance with the carbon metal arc experiments of Seraphin *et al.*, who pointed out that their chain structures could be found in high densities when the experimental parameters also favoured the production of fullerenes. However Seraphin *et al.* hypothesised that amorphous carbon was converted into graphitic layers at metal particle–carbon interfaces.[13] The growing stack would then remove itself from the interface and was closed up into a sphere, thus reducing the surface energy associated with an open structure. The newly generated graphitic particle joined the chain behind it and a new stack would begin to grow from the interface. This consecutive growth of the nanoparticles of one chain at a single metal particle was supported by their observation that often partly encapsulated metal particles were found at one end of a chain. Likewise, in our experiments all particles in a given chain were of almost the same size, which might be determined by the metal particle's diameter.

The multi-wall graphitic nature of the nanoparticles forming the chains is an indication that fullerenes reacted with metal particles in a similar way as gaseous carbon-containing compounds are supposed to do according to the VLS model. However, the precipitation of carbon was not continuous. Chains of multi-walled carbon nanoparticles were generated rather than MWCNTs. The reason for the oscillation of the tube formation reaction resulting in building chains of particles is probably melting and solidification of the catalytic metal particles: In the experiments with graphite, melting processes of the nickel and cobalt films were observed at temperatures close to the point where nanochain formation also took place with FB1. The dramatic decrease of the melting temperature can only be explained partly by the carbon content in the metals, which can reduce the melting temperatures for carbon–metal solutions to 1320 °C and 1327 °C for nickel and cobalt respectively.[23] A further effect is certainly caused by the high amount of surface energy of the small metal aggregates. This phenomenon can cause surface melting[30] even below the typical drastically reduced melting temperatures of small metal particles.[31–33]

Since above 850 °C the structure of the nanochains was not dependent on the oven temperature, it is likely that the reaction always took place at the same temperature (about 800 °C): When the FB1 pellets were inserted into the hot oven, they were heated rapidly. At a certain temperature the fullerenes became effectively evaporated, an endothermic process, which inhibited a further rapid temperature increase. A fast growth process is also supported by the fact that the structures built up were not dependent on the pyrolysis time above 1 min.

The preliminary results of the reaction of C_{60} vapour with laser-deposited nickel films show that there is a temperature window between 800 and 1000 °C where fibre formation takes place. The lower limit is most likely set by the vapour pressure of C_{60}. The upper temperature limit can be explained by the observations of the nickel and cobalt films on glassy carbon: At moderate temperatures the glassy carbon was transformed into polycrystalline graphite, indicated by the intensive roughening. At higher temperatures the metal films melted, formed big droplets and lost effective contact with the substrate due to their surface tension.[26] In this way it was impossible to absorb enough carbon to reach supersaturation on the time scale of the reaction, which would have resulted in the precipitation of graphite. This loss of contact or the large size of the melted particles are probably the reasons why nanochains could not be produced with cobalt. The homogeneous melting model[31] predicts slightly lower melting points for small carbon-containing cobalt particles with the eutectic composition than for carbon-containing nickel particles of the same size, if the reaction enthalpy of the decomposition of the fullerene vapour is taken into consideration.[29] So the cobalt particles may melt completely under the reaction conditions below the lower temperature limit set by the fullerene evaporation and form inactive droplets. The melting and droplet formation of nickel is most likely the reason why we observed in our laser experiments an upper limit of 1000 °C for the formation of nanochains. The existence of an upper temperature limit for the formation of the chain structures was indicated by Seraphin *et al.*[13] They found especially enriched chains of nanoparticles in the peripheral parts of the cathode deposit. Therefore moderate rather than high temperatures did promote nanochain growth.

The production of low densities of fibrous material on the nitrogen-containing fullerene black FB4 with nickel and cobalt films therefore indicates that carbon-containing gases (cyanogen?) were evaporated and reacted at low temperatures before the metal films could melt.

Molybdenum did not promote the generation of the carbon nanoparticles like nickel did. The high melting point (2617 °C) implies that the diffusion of carbon through this metal in the temperature range up to 1200 °C is quite small. Moreover the phase diagram for a carbon–molybdenum system shows that the molybdenum is likely to be converted into the carbide (MoC) before any graphite can be produced from carbon-containing gases at temperatures below 1220 °C.[23] This carbide formation step requires a huge amount of carbon, probably more than provided in our experiments. In the case

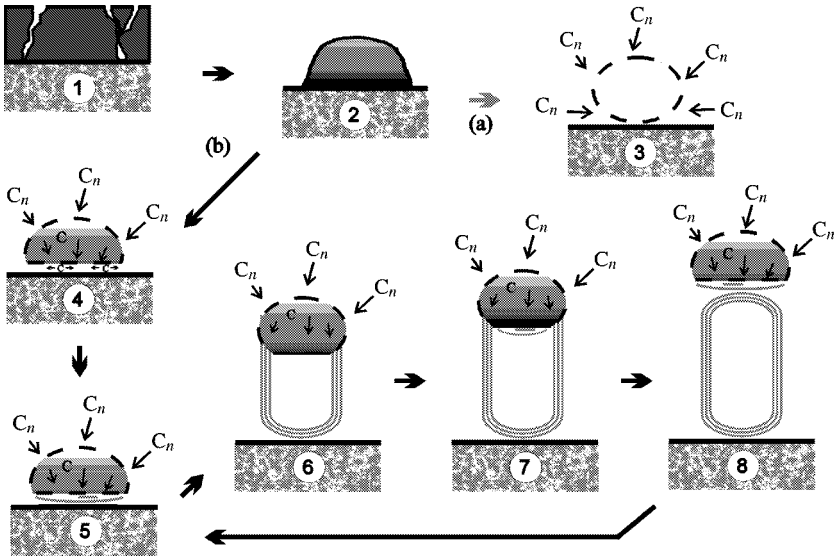

Fig. 7 Possible mechanism of nanochain formation, metal: dark → cold, light → hot, dashed line → molten surface, solid line → solid surface.

of nickel, any involvement of carbides in the formation of hollow nanoparticles can be ruled out as the metastability region for nickel carbide extends only up to a temperature below 450 °C.[24,25,29]

5. Possible growth model for carbon nanochain formation

Our ideas are sketched in a scheme (Fig. 7), which was partially adapted from the VLS model.[20]

(1)–(2) Heat converts the polycrystalline metal film into metal islands.

(2)–(3) Exothermic decomposition and absorption of fullerenes can cause the metal to melt, creating inactive droplets (a). This is hypothesised for cobalt films even at moderate and for nickel films only at higher temperatures.

(2)–(4) Alternatively, the diluted carbon may only cause surface melting of the particle (b). Carbon diffuses into the cooler regions near the substrate, where supersaturation leads to the segregation of carbon. More carbon can be stored in a molten than in a solid phase.

(4)–(5) Graphitic planes are precipitated parallel to the particle surface.[14,26] The first plane grows until it covers the contact surface of the particle with the substrate.[17] Subsequent planes bend the previous one. The bending of the planes will stabilise the unsaturated sp^2 orbitals of the edge of the graphene sheets due to the overlap with the d orbitals of the metal.

(5)–(6) This contact then serves as a crystallisation seed for the following segregation of carbon, initialising cylindrical growth.

(6)–(7) The surface of the whole system grows as the reaction continues. The increased surface intensifies the cooling of the particle from the surrounding gas atmosphere and through radiation. This may cause the interface between metal and carbon fibre to solidify. Solidification leads to the rapid segregation of carbon atoms, which build up planes inside the contact circle of the tube and the catalytic particle.

(7)–(8) The new graphitic planes will close the previously built multi-wall cylinder. Excess planes will serve as the starting point for the next nano-unit to be formed in the same way.

6. Conclusions

We have generated chains of hollow, elongated graphitic nanostructures from a fullerene black by simply heating the samples in the presence of thin nickel films. It was proved that gaseous fullerenes are the feedstock for the formation of the nanochains. We adapted the diffusion model for the formation of MWCNTs to our findings and propose that repeated surface melting and solidification of the catalytic metal particle may be the reason for the oscillation of the reaction.

Acknowledgements

This work has been funded by the German Ministry of Science and Technology and the SFB 337. We received helpful information about cluster melting from Prof. H. Haberland, Freiburg, and thank H. Kraß and O. Pyper, Berlin, for fruitful discussions. We also thank Degussa-Huels AG for supplying us with carbon black samples.

References

1 W. Krätschmer, L. D. Lamb, K. Fostiroupolos and R. D. Huffman, *Nature*, 1990, **347**, 354.
2 D. H. Parker, P. Wurz, K. Chatterjee, K. R. Lykke, J. E. Hunt, M. J. Pellin, J. C. Hemminger, D. M. Gruen and L. M. Stock, *J. Am. Chem. Soc.*, 1991, **113**, 7499.
3 T. Belz, J. Find, D. Herein, T. Rühle, H. Werner, M. Wohlers and R. Schlögl, *Ber. Bunsen-Ges. Phys. Chem.*, 1997, **101**, 712.
4 S. Iijima and T. Ichihashi, *Nature*, 1993, **363**, 603.
5 D. S. Bethume, C. H. Kiang, M. S. de Vries, G. Gorman, R. Savoy, J. Vazquez and R. Beyers, *Nature*, 1993, **363**, 605.
6 Y. Saito, M. Okuda, N. Fujimoto, T. Yoshikawa, M. Tomita and T. Hayashi, *Jpn. J. Appl. Phys.*, 1994, **33**, L526.
7 T. Guo, P. Nikolaev, A. Thess, D. T. Colbert and R. E. Smalley, *Chem. Phys. Lett.*, 1995, **243**, 49.
8 A. Maiti, C. Brabec, C. Roland and J. Bernholc, *Phys. Rev. B*, 1995, **52**, 4850.
9 Y. H. Lee, S. G. Kim and D. Tománek, *Phys. Rev. Lett.*, 1997, **78**, 2393.
10 J.-C. Charlier, A. De Vita, X. Blase and R. Car, *Science*, 1997, **275**, 646.
11 H. Kanzow and A. Ding, *Phys. Rev. B*, 1999, **60**, 11180.
12 Y. Saito, T. Yoshikawa, M. Okuda, N. Fujimoto, K. Sumiyama, K. Suzuki, A. Kasuya and Y. Nishima, *J. Phys. Chem. Solids*, 1993, **54**, 1849.
13 S. Seraphin, S. Wang, D. Zhou and J. Jiao, *Chem. Phys. Lett.*, 1994, **228**, 506.
14 T. Baird, J. R. Fryer and B. Grant, *Nature*, 1971, **233**, 329.
15 R. T. K. Baker, M. A. Barber, P. S. Barber, P. S. Harris, F. S. Feates and R. J. Waite, *J. Catal.*, 1972, **26**, 51.
16 A. Oberlin, M. Endo and T. Koyama, *J. Cryst. Growth*, 1976, **32**, 335.
17 G. G. Tibbetts, *J. Cryst. Growth*, 1984, **66**, 632.
18 K. Hernadi, A. Fonseca, P. Piedigrosso, M. Delvaux, J. B. Nagy, D. Bernaerts and J. Riga, *Catal. Lett.*, 1997, **48**, 229.

19 N. M. Rodriguez, *J. Mater. Res.*, 1993, **8**, 3233.
20 R. S. Wagner and W. C. Ellis, *Appl. Phys. Lett.*, 1964, **4**, 8.
21 S. H. Irons, N. I. Nemchuk, H. W. Rohrs, T. Kowalewski, B. O. Faircloth, R. R. Krchnavek and R. S. Ruoff, in *Recent Advances in the Chemistry and Physics of Fullerenes and Related Materials*, ed. R. S. Ruoff and M. Kadish, Electrochemical Society Proceedings, 1997, vol. 97–14, p. 875.
22 N. Grobert, M. Terrones, A. J. Osborne, H. Terrones, W. K. Hsu, S. Trasobares, Y. Q. Zhu, J. P. Hare, H. W. Kroto and D. R. M. Walton, *Appl. Phys. A*, 1998, **67**, 595.
23 T. B. Massalski, *Binary Alloy Phase Diagrams*, ASM International, Materials Park, OH, 1996.
24 D. L. Leslie-Pelecky, X. Q. Zhang, S. H. Kim, M. Bonder and R. D. Rieke, *Chem. Mater.*, 1998, **10**, 164.
25 T. J. Konno and R. Sinclair, *Acta Metall. Mater.*, 1994, **42**, 1231.
26 R. Lambert, N. Jaeger and G. Schulz-Ekloff, *Surf. Sci.*, 1988, **197**, 402.
27 T. Belz, Thesis, Technische Universität Berlin, 1998.
28 R. F. Egerton, *Electron Energy-Loss Spectroscopy in the Electron Microscope*, Plenum Press, New York, 2nd edn., 1996.
29 H. Kanzow, Thesis, Technische Universität Berlin, 2000.
30 K. F. Peters, Y.-W. Chung and J. B. Cohen, *Appl. Phys. Lett.*, 1997, **71**, 283.
31 K. F. Peters, J. B. Cohen and Y.-W. Chung, *Phys. Rev. B*, 1998, **57**, 13430.
32 T. Castro, R. Reifenberger, E. Choi and R. P. Andres, *Phys. Rev. B*, 1990, **42**, 8548.
33 M. Schmidt, R. Kusche, W. Kronmüller, B. von Issendorff and H. Haberland, *Phys. Rev. Lett.*, 1997, **79**, 99.
34 W. Weisweiler, *Ber. Deut. Keram. Ges.*, 1971, **48**, 519.